Incorporating seismic horizons in inversion of CSEM data

Kristian Rymann Hansen* and Rune Mittet, Electromagnetic Geoservices ASA

SUMMARY

To improve the interpretation of controlled-source electromagnetic (CSEM) data it is desirable to include information from seismic data in a joint interpretation. The higher resolution of the seismic image makes it possible to accurately determine the depth of resistivity contrasts detected by the CSEM data. In this paper we show how horizons derived from seismic data can be incorporated in a CSEM inversion workflow to obtain resistivity models which are more consistent with both the CSEM data and the seismic data, and we demonstrate this workflow on a CSEM field data set.

INTRODUCTION

In recent years, the marine controlled-source electromagnetic method, also known as seabed logging (SBL) (Eidesmo et al., 2002), has proven a valuable tool for offshore hydrocarbon exploration. In marine CSEM a horizontal electric dipole is towed above the sea floor while a number of receivers record the low frequency response from the subsurface. The strength of the method lies in its ability to detect thin resistive layers associated with hydrocarbon reservoirs which contrast the typically more conductive formation.

To overcome the strong attenuation of the electromagnetic field in the conductive subsurface, the method relies on low frequencies (typically from 0.1 Hz to 10 Hz) which limits the resolution of the method. Furthermore, many inversion algorithms used for aiding the interpretation of CSEM data employ some form of smoothing regularization, producing models with highly smoothed resistivity boundaries. While several regularization methods exist that try to preserve sharp resistivity contrasts in the inversion result (Portniaguine and Zhdanov, 1999), these methods cannot overcome the limitation on the resolution of the CSEM method, and hence the precise location of any sharp resistivity boundaries remains uncertain.

To improve the interpretation of CSEM data, information from seismic data can be included in an inversion of the CSEM data. The higher resolution of the seismic image makes it possible to accurately determine the location of potential resistivity contrasts. A simple way of incorporating seismic horizons in a CSEM inversion is to divide the resistivity model into large volumes of homogeneous resistivity where the shape of the volumes are obtained from the seismic. Although this method can be useful, it can also lead to over-constraining of the inversion if not applied carefully, as discussed by Plessix and van der Sman (2008).

In this paper we propose a different method for incorporating seismic horizons in CSEM inversion through the use of regularization. This method has the advantage of not imposing hard spatial constraints on the inversion which reduces the risk of over-constraining. To demonstrate our method we apply it to a CSEM field data set, and since the survey consists of a single line of receivers, we employ a 2.5D inversion algorithm to invert the CSEM data. The 2.5D inversion has the advantage of being significantly faster than a full 3D inversion (Zach et al., 2008) but more accurate than a fast CMP inversion (Mittet et al., 2008), and thus provides a good compromise between speed and accuracy.

THEORY

In a 2.5D inversion algorithm it is assumed that a 2D resistivity model, in which the resistivity is invariant in the horizontal direction perpendicular to the towline, provides an adequate approximation to the real 3D subsurface. This is often a valid approximation when inverting CSEM data from a single towline, since the sensitivity to variations in resistivity in the transverse direction is limited (Tehrani and Slob, 2008). The advantage of the 2.5D approach is that the forward modeling algorithm used by the inversion is significantly faster than a 3D forward modeling code required for a full 3D inversion. Furthermore, the number of unknown parameters to be determined by the inversion algorithm is reduced, allowing the use of Hessian/Jacobian based parameter update algorithms. These algorithms have faster convergence than the gradient based methods typically used in 3D inversion (Nocedal and Wright, 2006).

From a given initial model, our inversion scheme employs a Gauss-Newton algorithm to minimize the standard cost function

$$E(m, m_{ref}) = E_D(m) + \lambda R(m, m_{ref}), \qquad (1)$$

The first term E_D is a weighted L_2 norm data misfit given by

$$E_D(m) = \sum_j \left| W_j \left(F_j^{obs} - F_j^{syn}(m) \right) \right|^2, \qquad (2)$$

where j is an index for a particular component of the electromagnetic field (e.g. the in-line horizontal electric field) at a given frequency and source/receiver position. The observed electromagnetic fields are denoted by F_j^{obs} and the corresponding synthetic fields for a given model m are denoted by $F_j^{syn}(m)$. W_j is the data weight for the corresponding data point and provides a measure of the uncertainty of the data point. The second term R in the cost function (1) is a regularization term which is required since the inverse CSEM problem is ill-posed. Both terms are functions of the model parameters m at a given iteration, while the regularization term also depends on a specified reference model m_{ref}. This reference model is the key to incorporating information obtained from seismic data into the CSEM inversion in our method. The regularization used in this work is a quasi-L_1 norm of the horizontal and vertical derivatives of the model parameters m, very similar to the one

used by Acar and Vogel (1994), and is given by

$$R(m, m_{ref}) = \alpha_x \int \sqrt{\left|\partial_x \left(m - m_{ref}\right)\right|^2 + \phi^2} dx dz$$
$$+ \alpha_z \int \sqrt{\left|\partial_z \left(m - m_{ref}\right)\right|^2 + \phi^2} dx dz, \qquad (3)$$

where α_x and α_z are weight factors for the horizontal and vertical spatial derivatives of the model, respectively, and ϕ is a focusing constant required to have well-defined derivatives of the regularization term for the Gauss-Newton algorithm. This type of regularization has the advantage of providing smooth solutions while also allowing for sharp resistivity contrasts in the model. The strength of the regularization is controlled by the scalar λ which is adjusted during the inversion in a manner very similar to the adaptive regularization discussed in (Zhdanov, 2002). Starting from a high value, λ is updated at every iteration according to the formula

$$\lambda_{n+1} = q\lambda_n, \qquad (4)$$

where n denotes the iteration number and q is a number between 0 and 1 controlling the rate of reduction of the regularization strength. When the data misfit term in the cost function (1) reaches a given target value, the value of λ is fixed at its current value until the inversion algorithm has reached a minimum of the cost function. This procedure ensures that a reasonable data fit is achieved without over-fitting the data.

Incorporating seismic horizons into CSEM inversion

We now describe our proposed method for incorporating information obtained from seismic data into an inversion of CSEM data. Starting from a very simple initial model containing only the sea floor topography along the towline, the water conductivity and a rough estimate of the background resistivity of the overburden, we first run an unconstrained inversion using our 2.5D inversion algorithm described above. The reference model in the regularization is the same as the initial model and thus contains no information on any resistivity boundaries except the expected resistivity contrast associated with the sea floor. The result of the unconstrained inversion gives an image of the background resistivity as well as any localized resistivity anomalies, but because of the aforementioned limitations on the resolution of the CSEM data, the boundaries between regions of different resistivity are generally not well resolved.

In the second step of our method, we compare the unconstrained inversion result to a seismic image acquired along the same line as the CSEM survey. From this comparison we can identify boundaries between the regions of different resistivity identified in the unconstrained inversion. We now construct a more detailed model of the background using the horizons from the seismic data and the background resistivity obtained from the unconstrained CSEM inversion. We use this model, which does not contain any localized resistive anomalies, as initial model and regularization reference model in a second CSEM inversion. Because we have included the reference model in the regularization term (3) of the cost function, the inversion will try to preserve the boundaries identified from the seismic, thus producing a model that is consistent with both seismic and CSEM data. We note that our method of including seismic information by using reference models does not

force the inversion to keep the boundaries included in the reference model, and the algorithm is free to remove or alter any such boundaries if this is required to fit the CSEM data. If a resistivity contrast is consistent with the CSEM data, our reference model will ensure that the boundary is consistent with the seismic image. Furthermore, we make no assumptions of homogeneity of any part of the model except the water column, which reduces the risk of over-constraining the model. As in all inversions, it is important to check that any model produced by the inversion gives a reasonable fit to the data.

CASE STUDY

We have applied our method to a field data set acquired in 2006 over a deep-water prospect in South-East Asia. 18 receivers recording the horizontal electric and magnetic fields were deployed along a line over the prospect with a separation of 1 km between receivers. The horizontal electric dipole source was towed along the line 30 m above the sea floor, emitting a square wave signal with a base frequency of 0.25 Hz, and with significant amplitude on the third (0.75 Hz) and fifth (1.25 Hz) harmonics. Except for the first receiver, which suffered technical difficulties and was therefore excluded from the inversion, the data quality of the receivers is excellent, allowing good data for the in-line electric field component to be obtained for offsets out to at least 10000 m, 7500 m and 5000 m for the first, third and fifth harmonics, respectively.

The initial resistivity model for the unconstrained 2.5D inversion consists of a water column and a homogeneous formation. Since the bathymetry is measured during the survey, our initial model has an accurate representation of the sea floor topography. The sea water resistivity is also measured directly and a value of 0.306 Ωm is used for the initial model, while the formation resistivity of the initial model is taken to be 2 Ωm. The unconstrained inversion converged after 90 iterations, obtaining a final average data misfit of approximately 10%, which was deemed adequate. To get a more detailed overview of the data misfit, we plot the quantity

$$\varepsilon(x_{cmp}, x_{off}) = \frac{\left|E^{obs}(x_{cmp}, x_{off}) - E^{syn}(x_{cmp}, x_{off})\right|^2}{\left|E^{obs}(x_{cmp}, x_{off})\right|^2} \qquad (5)$$

as a function of common midpoint (CMP) position $x_{cmp} = (x_s + x_r)/2$ and the absolute value of the half offset $x_{off} = |x_s - x_r|/2$, where x_s and x_r are source and receiver positions, respectively. E^{obs} and E^{syn} are the observed and synthetic electric field measurements sorted according to CMP position and offset. This data misfit plot for the base frequency (0.25 Hz) is shown in Figure 1 and shows that the largest data misfit is associated with short and long offset data. Disregarding the very long offset data, which is most affected by noise, we see that the data misfit is fairly evenly distributed among the CMP positions. This gives us confidence that our inversion result has not failed to reproduce any significant subsurface resistivity anomalies.

The resulting model of the inversion is shown in Figure 2 superimposed on depth converted seismic data acquired along the same line as the CSEM survey. The model clearly shows
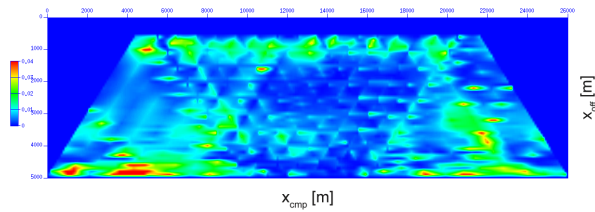
Figure 1: Data misfit plot for the base frequency (0.25 Hz) of the unconstrained inversion result.
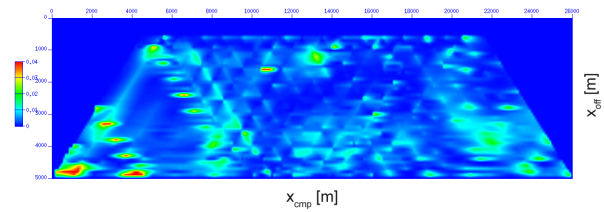

Figure 4: Data misfit plot for the base frequency (0.25 Hz) of the inversion with the seismic horizon included in the regularization reference model.

a resistive anomaly (red) associated with the seismic flat spot between 9500 m and 12000 m horizontal distance and approximately 2000 m below the sea surface. The lateral extent of the resistive anomaly matches quite well with the extent of the seismic anomaly, but the thickness of the reservoir is somewhat overestimated. The additional resistive anomalies seen just below the sea floor are most likely due to gas hydrates, which are known to be present in the area. As for the background resistivity, we identify two distinct regions of different resistivity. The overburden is seen to have a resistivity of approximately 3 Ωm (green), while the underlying formation has a lower resistivity of approximately 1.5 Ωm (light blue). We associate the transition from high to low resistivity with the very clear horizon seen in the seismic image around 2000 m below the sea surface. We note that while the transition from high to low resistivity occurs at approximately the correct depth, it does not accurately follow the seismic horizon. This is an effect of the limited resolution of the CSEM data. We also note that while the result of the unconstrained inversion provides a geologically reasonable model, there are a few features of this model that we consider to be inversion artifacts. The first is the presence of a low-resistivity region in the overburden between 9000 m to 13000 m in the horizontal direction above the reservoir anomaly. A large part of this anomaly is above the anticline structure seen between 10000 m and 14000 m in the horizontal direction. We see that in this area the consistency between the background resistivity distribution of the unconstrained inversion result and the seismic image is poor, and this may be the reason for the low-resistive anomaly in the otherwise resistive overburden. The second unphysical feature is the presence of the very small resistive anomalies seen below the first few receivers. These receiver imprints are most likely an artifact of the inversion, caused by the high sensitivity directly below the receivers.

Using the seismic and the unconstrained inversion result as a guide, we created a new model which contains an accurate boundary, derived from the seismic image, between the high resistive (3.2 Ωm) overburden and the low resistive (1.5 Ωm) underlying formation, but no resistive anomalies (see Figure 3). This model was then used as initial and reference model in a subsequent 2.5D inversion of the CSEM data. The inversion converged after 44 iterations with a final average data misfit of approximately 9%, slightly better than what was obtained in the unconstrained inversion. The data misfit plot shown in Figure 4 confirms that the data misfit is fairly evenly distributed among the data points.

The resulting model is shown superimposed on the seismic image in Figure 5. The result is quite consistent with the unconstrained inversion result shown in Figure 2, but the boundary between the resistive overburden and the underlying formation is now much more consistent with the seismic image. We also see that the unphysical features identified in the unconstrained inversion result are not present, confirming our suspicion that these were indeed inversion artifacts. Most likely, the improved consistency between the background resistivity distribution and the seismic image, included in the inversion via the reference model, has made these artifacts disappear.

CONCLUSIONS

We have presented a method for including information obtained from seismic data in inversion of CSEM data. Our method can be summarized as follows:

- First, an unconstrained inversion is performed.
- Regions of different background resistivity and their boundaries are identified from a joint interpretation of the unconstrained CSEM inversion and the seismic data.
- This information is then used to create an improved model of the background resistivity distribution.
- A subsequent inversion of the CSEM data is carried out using the improved background model as initial model and also as a reference model in the regularization.

The method has the advantage of not imposing hard spatial constraints and is therefore much less likely to over-constrain the inversion. We have applied our method to a field data set, producing a model which is more consistent with both seismic and CSEM data compared to the unconstrained inversion.

ACKNOWLEDGMENTS

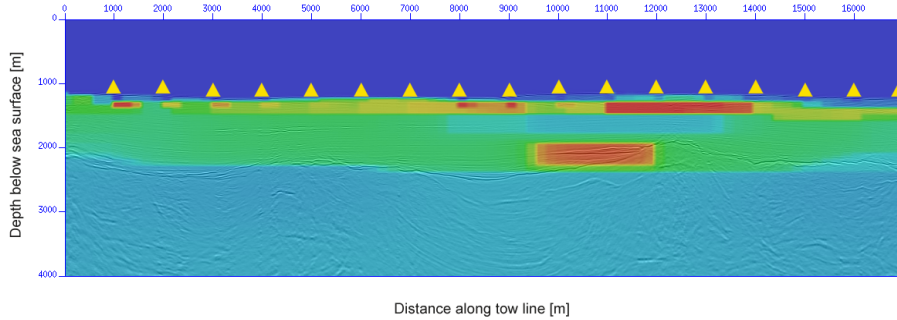We thank EMGS and Murphy Oil Corporation for permission to publish the results.

Figure 2: Result of the unconstrained CSEM inversion superimposed on the depth converted seismic image. The resistivity of the overburden is approximately 3 Ωm (green) and the resistivity of the underlying formation is approximately 1.5 Ωm (light blue). The boundary is clearly associated with the strong seismic horizon. A resistive anomaly (red) is associated with the seismic flat spot. The shallow resistive anomalies are likely due to gas hydrates. The receiver positions are indicated by the yellow triangles.
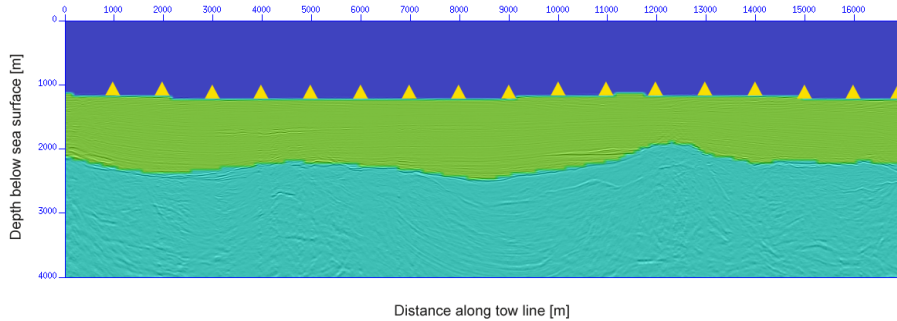

Figure 3: Reference model containing the horizon derived from the seismic image. The overburden resistivity is 3.2 Ωm and the underlying formation resistivity is 1.5 Ωm.
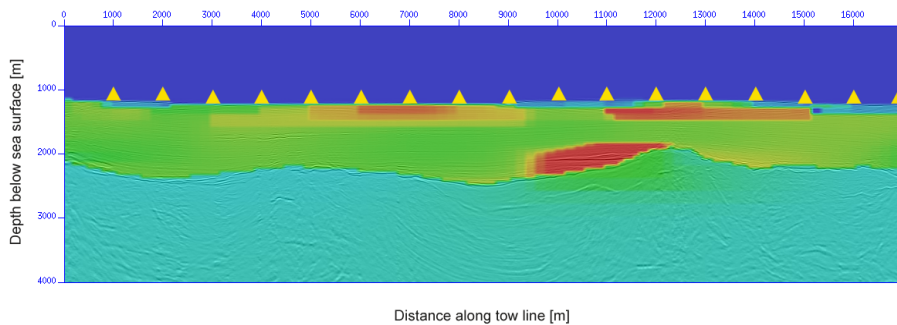

Figure 5: Result of the inversion with the seismic horizon included in the regularization reference model. The result is more consistent with the seismic image and has fewer inversion artifacts.

EDITED REFERENCES

Note: This reference list is a copy-edited version of the reference list submitted by the author. Reference lists for the 2009 SEG Technical Program Expanded Abstracts have been copy edited so that references provided with the online metadata for each paper will achieve a high degree of linking to cited sources that appear on the Web.

REFERENCES

Acar, R., and C. R. Vogel, 1994, Analysis of total variation penalty methods: Inverse Problems, **10**, 1217–1229.

Eidesmo, T., S. Ellingsrud, L. M. MacGregor, S. Constable, M. C. Sinha, S. Johansen, F. N. Kong, and H. Westerdahl, 2002, Sea bed logging (SBL), a new method for remote and direct identification of hydrocarbon filled layers in deepwater areas: First Break, **20**, 144–152.

Mittet, R., K. Brauti, H. Maulana, and T. A. Wicklund, 2008, CMP inversion and post-inversion modeling for marine CSEM data: First Break, **26**, 59–67.

Nocedal, J., and S. J. Wright, 2006, Numerical optimization: Springer.

Plessix, R. E., and P. van der Sman, 2008, Regularized and blocky 3D controlled source electromagnetic inversion: Progress in Electromagnetics Research Symposium Proceedings, 149–154.

Portniaguine, O., and M. S. Zhdanov, 1999, Focusing geophysical inversion images: Geophysics, **64**, 874–887.

Tehrani, A. M., and E. Slob, 2008, Modeling in-line data for seabed logging with 2.5D and 3D integral equations: 78th Annual International Meeting, SEG, Expanded Abstracts, 706–710.

Zach, J. J., A. K. Bjørke, T. Støren, and F. Maaø, 2008, 3D inversion of marine CSEM data using a fast finite-difference time-domain forward code and approximate Hessian-based optimization: 78th Annual International Meeting, SEG, Expanded Abstracts, 614–618.

Zhdanov, M. S., 2002, Geophysical inverse theory and regularization problems: Elsevier.